CHEMPHYSCHEM

ChemPubSoc Europe

DOI: 10.1002/cphc.201100986

VIP

STED Microscopy and its Applications: New Insights into Cellular Processes on the Nanoscale**

Tobias Müller, Christian Schumann, and Annette Kraegeloh*[a]

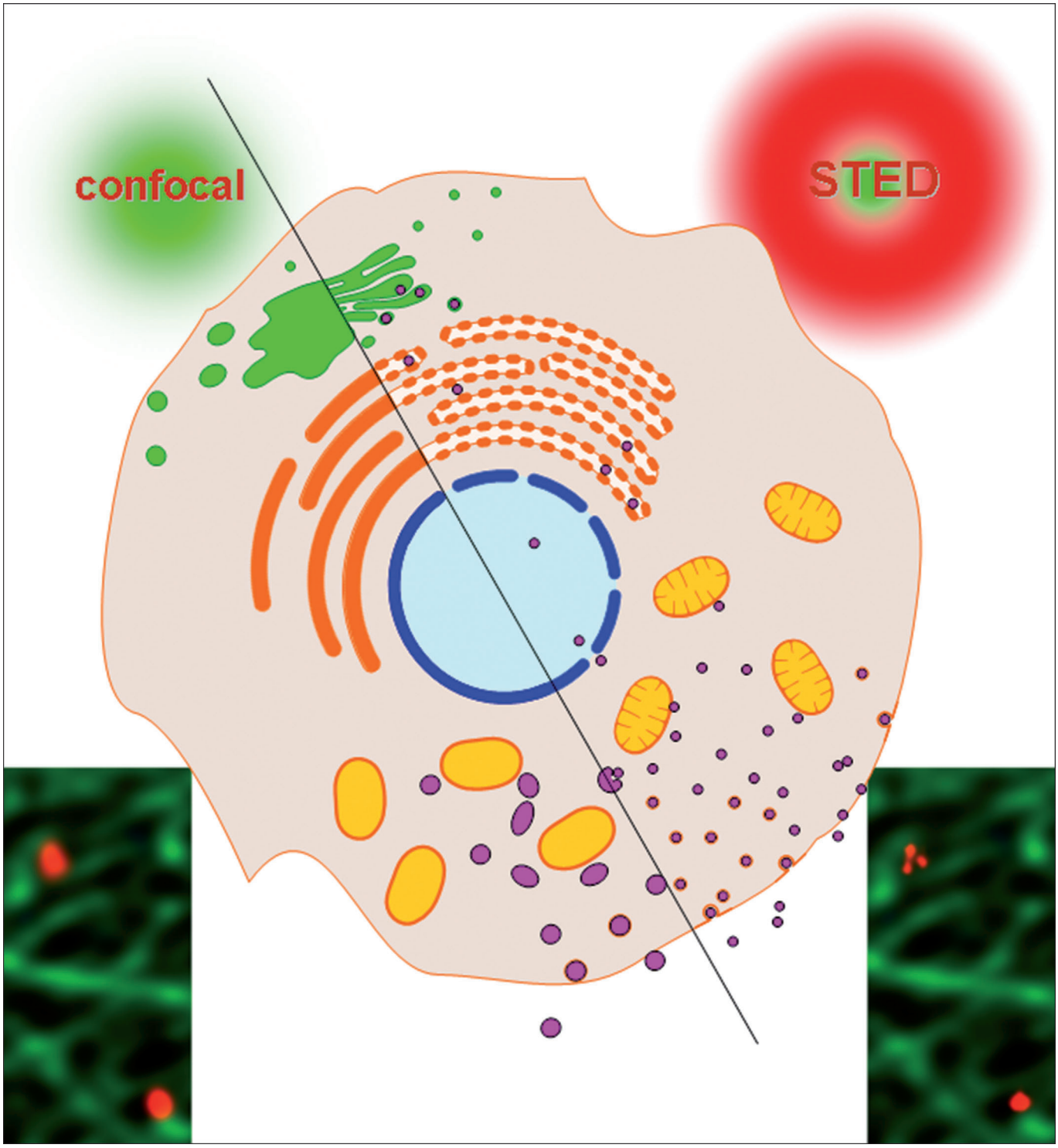

For about a decade, superresolution fluorescence microscopy has been advancing steadily, maturing from the proof-of-principle stage to routine application. Of the various techniques, STED (stimulated emission depletion) microscopy was the first to break the diffraction barrier. Today, it is a prominent and versatile form of superresolution light microscopy. STED microscopy has shed a sharper light on numerous topics in cell biology, but also in material sciences. Both disciplines extend into the nanometer range, making detailed studies of structural and functional relationships difficult or even impossible to achieve using diffraction-limited microscopy. With recent advancements like spectral multiplexing or live-cell imaging, STED microscopy makes nanoscale materials and components of the cell accessible for fluorescence-based investigations. With multicolor superresolution imaging, even the interactions between biological and engineered nanostructures can be studied in detail. This review gives an introduction into the working principle of STED microscopy, provides a detailed overview of recent advancements and new techniques implemented for use with STED microscopy and shows how these have been applied in the life sciences and nanotechnologies.

1. Introduction

Fluorescence microscopy has become an invaluable tool in biological investigations, both on a structural and on a functional level.[1] A vast array of labeling methods enable the specific attachment of fluorophores, fluorescent reporter molecules, to structures of interest in fixed and living biological systems.[2] Even more information on biological functions can be gained by the spatiotemporal observation of living specimens. Here, the large penetration depth, relatively low damage potential, compatibility with physiological imaging conditions and relatively easy sample preparation make optical far-field fluorescence microscopy the method of choice for all but very few biological applications. The availability of genetically encoded fluorophores adds even more to this advantage.[3]

For structural investigations, the width of the electromagnetic spectrum opens the possibility to use several spectrally distinct fluorophores to label and visualize different structures simultaneously within one specimen. The distribution of proteins and their spatial correlations in fixed specimens can give important clues to functional interactions. Since in biology the aspects of structure and function are linked inseparably on multiple levels of detail, this property is especially important because it allows elucidating structural/functional interdependencies. Ultimately, light microscopy serves to directly observe the processes by which a cell facilitates its numerous structural, mechanical and metabolical tasks. The use of fluorophores with narrow emission spectra, together with spectral unmixing,[4] has even allowed for the simultaneous detection of up to seven different fluorophores.[5]

Furthermore and of equal importance, multi-color light microscopy allows a direct view on cellular reactions to engineered materials. Especially fluorescent nanoparticles and their interactions with cellular structures attract growing attention as numerous applications introduce nanoscale materials into the environment.[6–8] Being of sub-diffractional size, both nanoparticles and their cellular interaction partners benefit from the recent developments in fluorescence microscopy that are pushing the resolution limit down to the nanoscale.

2. Advances in Fluorescence Microscopy

An important step in the evolution of modern optical imaging has been the introduction of confocal optics and the confocal laser scanning microscope.[9,10] (Figure 1) In this method, a diffraction-limited excitation spot within the specimen is imaged onto a confocal aperture, which is positioned in front of a point detector. The confocal aperture rejects light from neighboring focus planes, and for imaging the focal spot is scanned across the specimen. This concept of axial restriction of the optical detection volume has not only enabled real 3D imaging, but has also introduced the notion of an optically confined micro-cuvette within the specimen. This cuvette formed by the detection volume allows the usage of fluorescence spectroscopic methods to gain spatially resolved insight into biochemical dynamics, beyond the pure optical imaging. The spectroscopic methods implemented in modern confocal microscopes encompass among others time-resolved spectroscopy (FLIM, fluorescence lifetime imaging),[9,11] photoselection and polarization anisotropy measurements,[12] and fluorescence correlation spectroscopy.[13,14] One of the main obstacles in optical imaging has long been the effect of diffraction, limiting the resolution to approximately half the wavelength of the light used. The use of UV and shorter wavelength light is limited by the concomitant ionization and radiation damage of fluorophores as well as living specimens. In the last decade, this resolution limit has been overcome by a number of diffraction-unlimited optical imaging techniques.

Most of these superresolution techniques can be categorized into two groups.[15] In stochastic superresolution microscopy, the single-molecule nature of the fluorescent emitters together with random switching schemes is exploited to determine their position much more precisely than the optical resolution of the instrument. To enable a precise localization, only one single emitter is allowed to emit per area determined by the diffraction-limited resolution. In order to achieve this behavior, several molecular switching methods based on switchable fluorescent proteins (PALM, photoactivation localization microscopy),[16] organic dye pairs (STORM, stochastic optical reconstruction microscopy)[17] and light-induced ground-state depletion (GSDIM: ground-state depletion followed by individual

[a] *Dr. T. Müller,[+] Dr. C. Schumann,[+] Dr. A. Kraegeloh*
INM-Leibniz-Institute for New Materials
Nano Cell Interactions Group
Saarbrücken (Germany)
E-mail: annette.kraegeloh@inm-gmbh.de

[+] *These authors contributed equally to the work.*

[**] *STED: Stimulated Emission Depletion*

molecule return, dSTORM: direct stochastic optical reconstruction microscopy)[18,19] have been developed. The detection of a sufficiently large number of single-molecule events allows the pointillistic reconstruction of the fluorophore distribution by fitting of the respective centers of the single-molecule events. The technique of spectrally assigned localization microscopy is conceptually similar to the aforementioned methods.[20]

Most of the non-stochastic superresolution techniques are defined by point spread function (PSF) engineering. The PSF represents the response of the optical imaging system to a single infinitely small emitter, and is thus a direct representation of the optical resolution of the system. Among the PSF engineering methods, structured illumination (SIM)[21–23] uses a spatially modulated illumination pattern along with mathematical reconstruction to double the bandwidth of the optical system, thus doubling its resolution. This bandwidth doubling is also the case for the ideal confocal microscope, where the spatially modulated illumination is achieved by the diffraction-limited excitation spot, and the real space resolution can be restored by deconvolution. A nonlinear extension of SIM is saturated structured illumination microscopy (SSIM),[24,25] where nonlinear saturation effects are exploited to increase resolution even further. These structured illumination techniques work in parallel by scanning the excitation pattern in the spatial frequency space and reconstructing the real space fluorophore distribution, in contrast to PSF engineering methods that reduce the size of the emitting fluorescent volume in real space. The PSF engineering methods commonly use point scanning, although parallelized implementations have been developed,[19,26,27] and schemes like slit scanning can be envisioned. Using a precise interpretation of the definition, 4Pi microscopy[28] is not diffraction-unlimited, but rather makes use of two opposing lenses to use the largest possible angular spectrum to increase the axial resolution of the scanned focal spot. In the RESOLFT (reversible saturable optical fluorescence transitions) concept[29–31] the fluorophores in the outer range of the scanned focal spot are prevented from fluorescence by local saturation of a molecular transmission, while the fluorophores at the spot center remain unaffected. This can be accomplished by ground state depletion (GSD)[32,33] that does not leave any molecules in the electronic ground state S_0 to be excited to the fluorescent S_1 state, as well as stimulated emission,[34–36] depleting the S_1 state and thus switching off the fluorescence capability of the fluorophores before fluorescence can occur (STED). One main advantage of point-scanning PSF engineering methods lies in the fact that the real physical volume of the PSF is reduced, so the concept of the optical micro-cuvette inside the specimen can be sustained. Furthermore, except for a deconvolution to reduce the effect of axial diffraction sidelobes in 4Pi microscopy, these techniques do not require any mathematical post-processing. Common to all RESOLFT concepts, by virtue of the optical switching of the saturable transition used to reduce the PSF volume, the resolution increase is easily accessible by means of the intensity of the laser driving the transition. In STED microscopy, this is the intensity of the depletion laser. By tuning this external parameter, the microscopist can adjust the focal spot size freely, sacrificing resolution if a stronger signal is needed or if bleaching is an important issue,[37] or contrarily maximizing resolution when working with optimal, bleach-resistant samples.[38]

The common feature of all superresolution methods is the molecular switching, which enables a temporally sequential imaging of emitters which would not have been separable when imaged simultaneously. The switching can be stochastic as in PALM/STORM/GSDIM or at predetermined positions as in STED/GSD/RESOLFT/SIM, and can be parallelized up to a certain limit. The parallelization is inherent in structured illumination methods, whereas stochastic schemes detect several fluorophores per image frame, and multi-focus methods can be

Tobias Müller graduated in biology at the University of Mainz (Germany) in 2003. He later went on to Göttingen (Germany) for his PhD thesis at the department of Stefan Hell at the Max Planck Institute for Biophysical Chemistry, working on 4Pi microscopy of intra-Golgi trafficking. Since 2011, he is a postdoctoral researcher at the *Nano Cell Interactions* group at the INM Leibniz Institute for New Materials in Saarbrücken (Germany). He is currently working on nanoparticle trafficking and import mechanisms, using superresolution STED microscopy.

Christian Schumann is a postdoctoral researcher at INM Leibniz Institute for New Materials in Saarbrücken (Germany). He graduated in physics at the University of Kaiserslautern (Germany) in 2004 and received his Ph.D. at the same university working on ultrafast visible and infrared spectroscopy of the primary reactions of biological photoreceptors in 2008. He joined the *Nano Cell Interactions* group at INM in 2009. His current research involves the application of advanced optical imaging techniques to the study of biological interactions of chemical nanomaterials.

Annette Kraegeloh studied biology in Bonn and Sydney and received her doctoral degree on osmoregulation and transport in halophilic bacteria. Since 2004 she has been affiliated to INM-Leibniz Institute for New Materials in Saarbrücken. She initially was engaged in nanomaterials for biomedical applications. Since 2008, as head of the *Nano Cell Interactions* group, she is concentrating on the interactions between engineered nanoparticles and human cells.

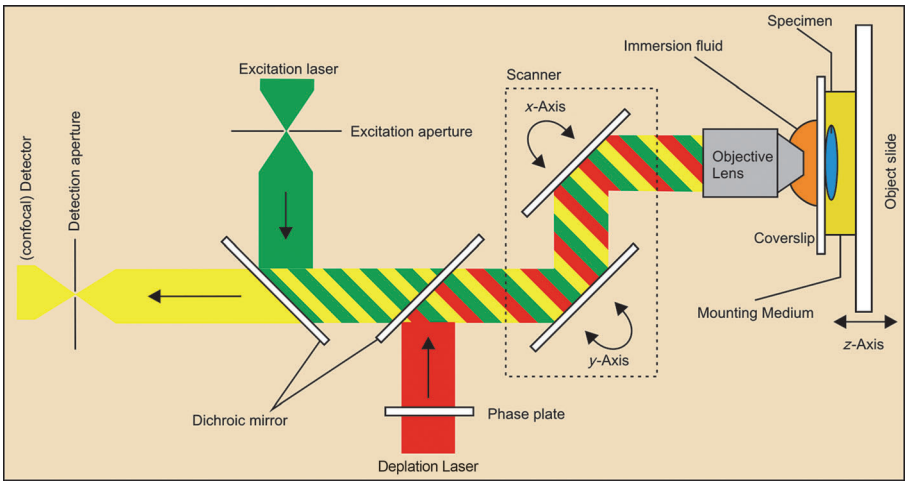

Figure 1. Optical path and location of the sample in a conventional laser scanning microscope. The laser beam scans the sample in *xy* direction first. The focal plane can be adjusted by variation of the distance between sample and objective (axial, along the *z*-axis). With a depletion laser, the configuration corresponds to a STED microscope.

employed in PSF engineering approaches.[26,27] Linear imaging schemes, such as conventional confocal microscopy or linear SIM are limited to the double bandwidth of a widefield microscope by using diffraction-limited excitation and detection. Superresolution methods with resolutions beyond double the diffraction-limited resolution all rely on nonlinear switching schemes, like saturable transitions or the highly nonlinear replacement with the center position of a localized spot.

3. The STED Principle

The basic idea behind STED microscopy as noted above is the spatially selective deactivation of fluorophores, preventing their participation in image formation. (Figure 2) The photophysics of the fluorescence process can be modeled as an excitation from the electronic ground state S_0 of the fluorophore to the excited singlet state S_1 induced by the excitation beam. Here, after initial vibrational relaxation, the fluorophore can emit light as fluorescence via spontaneous emission and return to a vibrationally excited substate of the S_0 electronic state. In a simple model, the energy lost in vibrational relaxation in this process can be viewed as the Stokes shift between excitation and emission spectrum. But spontaneous emission of fluorescence is not the only deactivation process of the S_1 state. Most importantly, an incident photon can initiate stimulated emission, in which a second photon is emitted. Here, the efficiency of the stimulated emission process is scaled by the number of incident photons. If only enough photons are incident on the fluorophore, the S_1 state can be depleted before a fluorescence process can occur, and fluorescence is thus prevented. This optically saturable process introduces the nonlinearity that is exploited to increase the resolution in STED microscopy by using high intensities for the depletion laser. (Figure 3) The wavelength of the stimulated emission can be chosen to be shifted to higher values relative to the maximum of the emission spectrum, and can hence be spectrally separated on the detection side.

The high laser intensities required for a complete depletion of the S_1 state in STED imaging also affect the photobleaching rate in the specimen,[39] not only in the image plane, but also in the light cone above and below the focal spot. To keep pho-

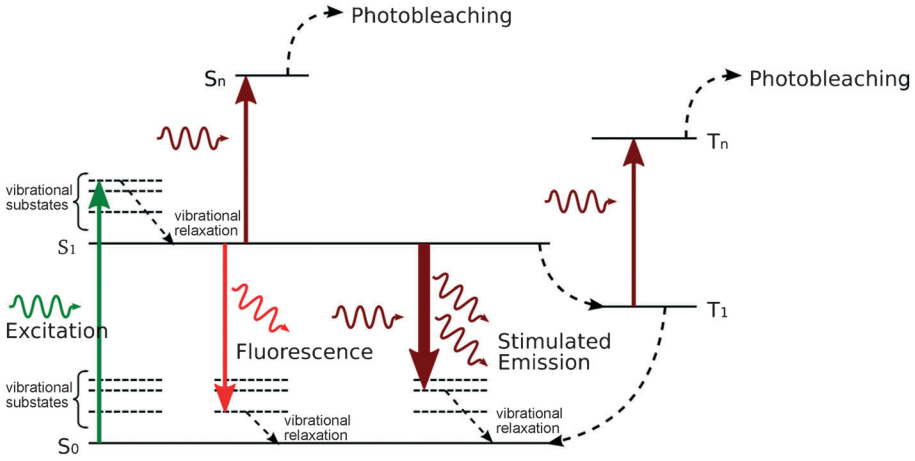

Figure 2. Simplified Jablonski diagram of the molecular states involved in STED imaging. After initial excitation from the S_0 to the S_1 state and vibrational relaxation, fluorophores can emit fluorescence photons. Alternatively, the fluorescence can be silenced by driving a stimulated emission transition into a higher vibrational substate of the electronic ground state S_0. The red-shifted stimulated emission light can be spectrally separated during detection. The bleaching pathways indicated in the diagram are addressed in the text.

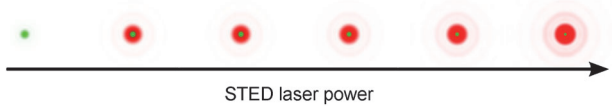

Figure 3. Reduction of lateral PSF size using STED with a doughnut-shaped depletion pattern (red). The diffraction-limited excitation pattern is depicted on the left. Starting with the second image from left to right, the depicted effective PSFs (green) result from a doubling of STED laser power from each image to the next.

tobleaching at a minimum, several concepts have been developed. The right choice of fluorophore can prevent photobleaching induced by absorption of the STED laser by the S_1 state and excitation into higher singlet states. To prevent this population of highly excited singlet states, the stimulated emission spectrum and excited state absorption spectrum of the fluorophore should not overlap.[40] To reduce photobleaching by excitation of long-living triplet states, either the repetition rate of the laser in a pulsed STED Scheme can be reduced to allow triplet state relaxation between two laser pulses,[41] or chemical reagents can be used to ensure a depletion of the triplet state through redox reactions.[42,43]

The spatial structure of the depleted area in which the fluorescence is switched off by stimulated emission can be engineered by using wavefront modifying elements in the pupil plane of the objective lens. Using high-aperture vectorial focusing calculations allows the design of diffractive optical elements (DOEs) for a variety of depletion patterns, including 1D and 2D lateral confinement and axial confinement, and combinations thereof.[44–46] (Figure 4) The most prominent example is the doughnut shape used for lateral confinement in 2D, which is generated by a helical phase ramp in conjunction with a circular polarization of the depletion laser beam. The lateral resolution of such an optical setup typically varies between 30 nm and 80 nm for biological samples, dependent on the properties of the sample and on the applied power of the depletion laser. In specific cases, values down to 6 nm lateral resolution have been achieved.[38] Using different depletion schemes, axial resolutions on the order of 100 nm have been demonstrated,[35] and even isotropic resolutions of 30 nm are possible.[47] In this context, the combination of STED and 4Pi imaging has also proven useful.[48] In order not to sacrifice signal photons from the actual imaging spot, the destructive interference of the depletion beam at the center of the excitation focus has to be near-perfect, imposing constraints on the optics used in such applications. Also, the registration of the excitation and depletion patterns, which are generated by laser beams of different wavelength, is crucial for a good signal ratio, resulting in requirements of the correction of the imaging optics.

Regarding the optical implementation of driving the molecular transitions involved in the STED principle, a number of concepts have been published. The first implementation was based on pulsed lasers, where the effective stimulated emission probability can be optimized by proper selection of delays between excitation and depletion pulses and the depletion pulse length.[35,41,49] This concept necessitates expensive lasers, so an implementation based on CW lasers was developed.[50] The broad range of strong continuous wave (CW) laser sources available as turn-key systems has widened the usability of such systems to end-users tremendously and has extended the wavelength and thus the fluorophore range available for benchtop systems. More recently, a two-photon process[51] for the excitation in STED imaging has been implemented,[52–55] exploiting the intrinsic optical sectioning of the two-photon excitation mode and allowing the use of non-descanned detection. Together with the demonstration of STED imaging with large penetration depth using appropriate optics,[56] it seems clear that the imaging depth of STED will be pushed further in the future.

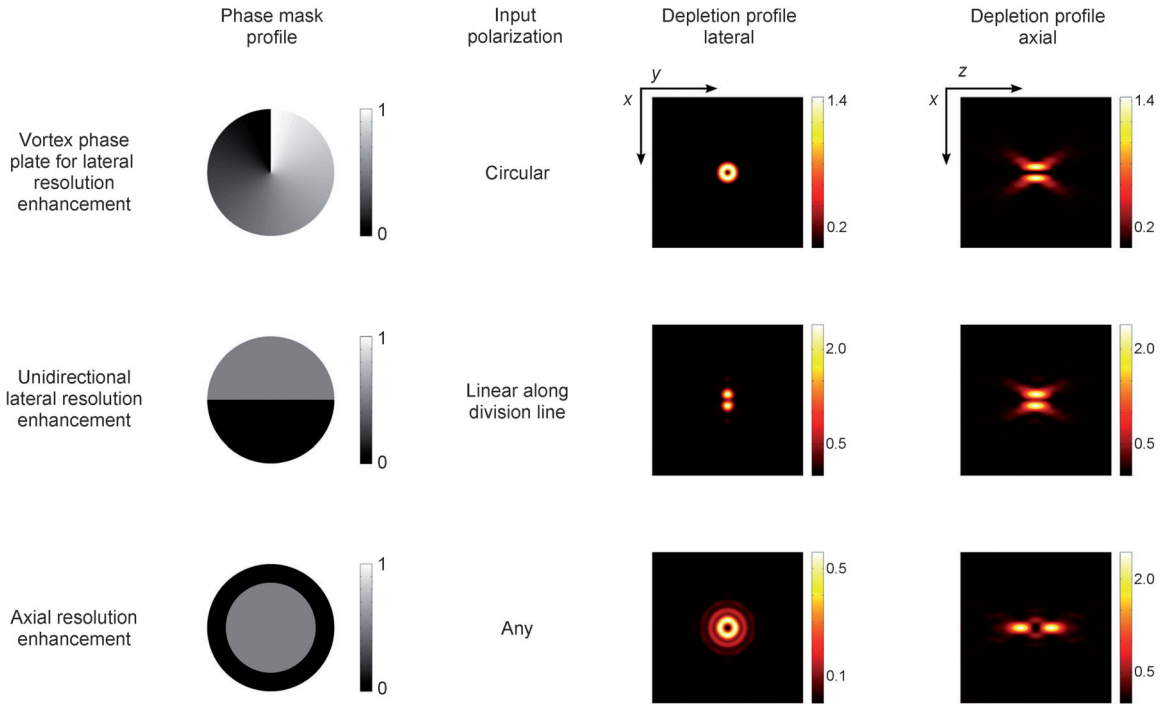

Figure 4. Phase masks (second column) commonly used in STED microscopy and corresponding depletion patterns (fourth column lateral section in the focal plane, fifth column axial section along the meridional plane). The optical thickness is given in units of depletion laser wavelengths. For the vortex phase ramp, strict circular polarization is required for the STED laser beam.

There are several concepts to transfer the spectral multiplexing property of conventional fluorescence imaging to STED imaging. These concepts encompass four-beam schemes[57,58] using separate excitation and depletion beam pairs for two fluorophores, schemes employing the same depletion beam for both fluorophores[59–61] and other concepts.[62,63] The rapid recent progress in this aspect of STED development will introduce multicolor STED imaging to a wider field of applications.

The reduction of the focal volume in STED microscopy reduces the number of fluorescent labels in that volume. Even though this reduces the apparent brightness of the specimen, it removes photons from adjacent positions, which is the core principle of the resolution improvement. In order to fulfill the Nyquist sampling criterion, smaller steps have to be used when scanning the specimen, leading to longer recording times if not compensated by reducing the field of view. Concomitantly, a lower number of detected photons per sample point also reduces the signal-to-noise ratio. To ensure high photon collection efficiencies, sensitive detectors like avalanche photodiodes are usually employed. New developments, such as gallium arsenide phosphite (GaAsP) hybrid detectors are also promising technologies, combining the high quantum efficiency of the avalanche process with increased dynamic range. Furthermore, the fast time response of avalanche photodiode (APD) detectors and GaAsP hybrid detectors allows for a time-resolved detection of photons. This enables the implementation of gated detection schemes,[64,65] which suppress background light as well as light from the outer range of the focal spot and thus increase resolution by exploiting the time characteristics of the molecular STED mechanism.

The purely physical and variable reduction of the focus volume in STED microscopy has been used to adapt fluorescence correlation spectroscopy to superresolution imaging.[66–68] In this application, STED microscopy not only allows the exploration of processes on a spatial scale beyond the diffraction limit, but also opens the possibility to address the technical problem of recording correlations in situations of high fluorophore concentration, such as overexpression of fluorescent protein constructs. Also, fluorescence lifetime imaging has overcome the diffraction limited resolution by implementation in a STED microscope.[69]

4. Dyes and Labeling Systems for STED Microscopy

At the beginning of STED applications, the range of dyes available for this technique was rather limited. In the first theoretical description of STED microscopy, Rhodamine B was named a potential STED dye.[34] The first dyes that were subsequently used for this newly developed technique were typical laser dyes emitting in the red spectral range. Examples are lipophilic pyridine dyes: Pyridine 2 embedded in fluorescent beads and Pyridine 4 used for labeling the membrane of bacterial cells (*Escherichia coli*). The styryl dye RH414 has been used to stain the vacuolar membrane of living yeast cells,[35] whereas JA 26 was applied after spin-coating on a glass surface.[70] In order to enable advanced biological imaging, the dyes have to be specifically targeted towards the structure of interest. In addition, further technical developments, for example, new laser sources, and novel applications, for example multi-color imaging and imaging of living cells using advanced labels, have motivated but also demanded a progressive expansion of dyes and labeling systems suitable for STED. Up to now, more than forty different fluorophores covering almost the entire visible spectrum have been applied for STED imaging (Table 1).

A breakthrough towards broader applicability of STED for cellular imaging was its utilization for immunolabeled cells. In the first description of this technique, the authors used the red-emitting dye MR-121SE coupled to an anti-mouse secondary antibody via amide bonds.[39] Currently, immunolabeling is the gold-standard for STED microscopy. It allows labeling of both structures in fixed and permeabilized cells and components that are expressed on the surfaces of living cells.[37] This technique is available for dyes that can be covalently coupled to antibodies and in STED microscopy has been applied to a broad range of dyes, for example green-emitting Atto 532[41,71,72] and Atto 565, yellow-emitting Atto 590, and red-emitting Atto 633.[73] A further example is the red-emitting dye Atto 647N that has been used for the first demonstration of two-color STED.[57] This dye is characterized by only minor excited state absorption competing with STED efficiency.[40] Dyes with a long Stokes shift like DY-485XL have been used for dual-color imaging using only one depletion laser.[59] Using orange Atto 590 together with Atto 647N and a second red-emitting dye called KK114 that has similar spectral properties, but a different fluorescent lifetime, STED has even been extended to three color imaging.[74] The library of dyes suitable for STED has recently been extended to the blue range using the dyes Atto 390 and Coumarin 102.[75] The design of novel dyes suitable for nanoscopy is an active field, aimed at developing dyes with high photostability, high fluorescence quantum yields, and low rates of transitions competing with stimulated emission.[40,76–78]

The specific targeting of fluorophores is fundamental for successful imaging strategies. As stated above, labeling approaches based on antibodies are restricted to non-living cells or labeling of cell surface structures that might subsequently be internalized by the cells. Therefore, labeling strategies have been developed that are better compatible with targeting intracellular or even cytosolic components. Such strategies comprise genetic engineering aimed at generating fusion proteins composed of the protein of interest and a labeling protein that are expressed by the cells. Widely used are autofluorescent proteins, which are available in a broad range of colors.[79,80] The first example of an autofluorescent protein for STED was the green fluorescent protein (GFP)[81] used to label virus derived particles and the Endoplasmic Reticulum (ER) of non-living cells.[82] The first example of fluorescent proteins used for STED imaging of living cells has been given by Hein et al.[83] In this study, the yellow fluorescent protein Citrine was targeted to the ER of mammalian cells. Nine consecutive images were recorded over 90 seconds, allowing the observation of structural changes of the ER network.[83] Time lapse STED imaging of dendritic spines of yellow fluorescent protein

Table 1. Fluorophores for STED microscopy.

Fluorophor	Absorption maximum [nm]	Emission maximum [nm]	STED wavelength [nm]	Additional information	References
Abberior STAR 440 SX	437[a]	515[a]	590–620	–	http://abberior.com
fluorinated rhodamines	512[b] 501[c] 552[d]	530[b] 524[c] 574[d]	590–620 595–615 645–665	rhodamine derivatives, uncaging at 360–440 nm	[78,165,166] http://abberior.com
Abberior STAR 635	635[b]	655[b]	740-760	rhodamine derivative	[76,77] http://abberior.com
Alexa Fluor 594	590	617	700 and 736	–	[54,167] http://invitrogen.com
Alexa Fluor 488	495	519	592	–	[168] http://invitrogen.com
Atto 425	436	484	532	coumarine like	[169] http://atto-tech.com
Atto 532	532	553	603	rhodamine like	[41,72,169] http://atto-tech.com
Atto 565	563	592	650–676	rhodamine like, two-photon excitation	[50,73,167,168,170] http://atto-tech.com
Atto 590	594	624	700	rhodamine like	[73,167] http://atto-tech.com
Atto 594	601	627	700	rhodamine like	[167] http://atto-tech.com
Atto 633	629	657	745–750	–	[73,171] http://atto-tech.com
Atto 647N	644	669	750–780	carborhodamine	[50,67,157] http://atto-tech.com
Atto 390	390	479	532	coumarine like	[75] http://atto-tech.com
B504-MA	514	530–540	592	Bodipy like	[60]
Chromeo 488	488	517	592	–	[168] http://activemotif.com
Chromeo 494	494	628	760	long stokes shift dye	[93] http://activemotif.com
Coumarin 102	400	480	532	–	[75]
DY-485XL	485[f]	560[f]	647	–	[59] http://dyomics.com
DY-495	493[f]	521[f]	592	fluorescein-based	[168] http://dyomics.com
DyLight 594	594[f]	615[f]	700	–	[167]
FITC	485	514	592	fluorescein- isothiocyanate	[168]
JA26	635	680	775–781	xanthene like	[70,172,173]
KK114	650	670	755	rhodamine like	[74,76,167]
MG-2p	632	664	730–750	Malachite green activated by L5-MG-L90S	[95,96]
MR 121 SE	532	700	793	oxazine like	[39]
Nile red	552[e]	636[e]	765	phenoxazine	[35] http://invitrogen.com
NK51	532	553	647	–	[59] http://atto-tech.com
Oregon Green 488	496	526	592	difluorofluorescein	[168] http://invitrogen.com
PTCA	458	530–540	592	Perylene like	[60]
Pyridine 4	550[f]	770[f]	765	–	[35]
Pyridine 2	500[f]	740[f]	765	–	[35]
RH 414	532[e]	716[e]	765	styryl dye	[35] http://invitrogen.com
TMR-Star	554	580	650	tetramethylrhodamine-derived, permeable	[92] http://neb.com
YOYO-1	491[g]	509[g]	568, 647	dimeric cyanine nucleic acid dye	[105] http://invitrogen.com
GFP	490	510	575	–	[82]
GFP switchable	488	511/515	595	Dronpa-M159T, Padron, on/off at 405 nm	[63]
YFP	514	527	598	–	[84]
Citrine	516	529	592	–	[83,174]
E2Crimson	611	646	760	tetrameric	[85]
TagRFP657	611	657	750	monomeric	[86]
NV diamond	532	600–850/685	775/740	fluorescent nitrogen vacancy centers	[38,98]
quantum dots	440 (excitation)	580	676	Mn-doped ZnSe	[97]

[a] in PBS, at pH 7.4, [b] in water, pH 7, [c] at pH7, [d] at pH 7.4, [e] in methanol, [f] in ethanol, [g] dye DNA complexes at pH 7.4. Additional information can be found in the list of dyes used in STED microscopy at http://www.mpibpc.mpg.de/groups/hell

(YFP) expressing neurons has also been performed using hippocampal slices from transgenic mice.[84]

More recently, also red-fluorescent proteins have been applied for STED. The first example is E2-Crimson, a derivative of the tetrameric protein DsRed-Express2.[85] In comparison to its parental protein, E2-Crimson exhibits red-shifted absorption and emission spectra allowing excitation with 635 nm.[85] The tetrameric structure of E2-Crimson favors its application as a label for luminal spaces of cellular organelles. A monomeric red-fluorescent protein called TagRFP657 with an even further

red-shifted emission maximum (657 nm)[86] was derived from the monomeric mKate.[87] In a first proof of concept, STED imaging was performed on fixed cells using TagRFP657 fusions to various cellular proteins.[86] In addition, reversible switchable fluorescent proteins (RSFPs), emitting at 515 nm have been used to image multiple structures in living cells, requiring only one excitation and STED wavelength and a single detection channel.[63]

A further approach that has been used to mark cellular components for STED is based on self-labeling proteins. Fused to the protein of interest, these proteins label themselves by binding of organic fluorophores. One example used for STED is a modified enzyme (haloalkane dehalogenase, HaloTag) that covalently binds to synthetic ligands.[88] These ligands consist of a reactive linker (chloroalkane) forming a covalent adduct with the HaloTag and a functional group, in this case a fluorescent dye (Atto 655) applicable for STED imaging.[89] Derivatives of the DNA repair protein O^6-alkylguanine-DNA alkyltransferase (SNAP-tag, CLIP-tag) that covalently bind fluorescently labeled derivatives of O^6-benzylguanine[90] or O^2-benzylcytosine[91] can be applied in a similar way.[92] Using the improved $SNAP_f$-tag and $CLIP_f$-tag as well as the dyes Chromeo 494 and Atto 647N, dual-color STED has recently been performed on living cells.[93]

One of the major advantages of self-labeling proteins compared to autofluorescent proteins is the applicability of organic fluorophores that exhibit higher extinction coefficients and quantum yields as well as a higher bleaching resistance. Their drawback is that many of the fluorophores suitable for STED are not membrane permeable[89,93] and thus not suitable for labeling of living cells. In addition, washing of samples is necessary to prevent background fluorescence. The development of wash-free labels might overcome this problem in future.[94]

In this aspect, fluorogen activating proteins might have superior properties, because they do not demand removal of unbound label. These reporter proteins are derived from human single chain antibodies[95] and bind fluorogens like malachite green with high affinity, thus increasing their fluorescence. STED imaging using such a reporter has been performed using fusions to cell surface bound receptors.[96] A further advantage of this system is that the label is bound non-covalently, thus during repeated scanning, exhausted labels might be replaced. A restriction in their use is that the fluorogens are not membrane-permeable and are known to be biological photosensitizers.

By now, a great range of labeling systems has been developed for various applications in fluorescence microscopy including STED. One aspect that is becoming increasingly important in the application high resolution microscopy is the physical size of the labeling systems themselves. Protein-based labels have molecular weights between 20 kDa and 50 kDa and a size of approximately 4–10 nm. Tuning the resolution towards the lower nanoscale range may eventually become limited by the size of the available labeling systems. Specific reporters with a low molecular weight might be advantageous, when ultra-high resolution is demanded. Ideally these molecules would be able to penetrate living cells, as this aspect still limits the applicability of nanoscopy to monitor dynamic processes inside living cells.

All of the dyes and labeling systems described so far are composed of organic compounds. Up to now, there are only two examples of inorganic fluorophores that have been used for nanoscale imaging according to the RESOLFT concept. The first example are quantum dots that have been optically switched off by excited state absorption.[97] The second example includes fluorescent nitrogen vacancy centers that have enabled the highest subdiffraction resolution thus far, reaching 6 nm in bulk diamond.[38] Such materials are even available in form of nanoparticles and have been imaged in cellular environment using a STED configuration.[98] Light-driven modulation of the fluorescence from Mn-doped ZnSe quantum nanocrystals has been established through excited-state absorption and its direct competition with spontaneous emission. Such optical control over electronic transitions enables far-field fluorescence microscopy analysis.

5. STED Applications

In recent years, STED microscopy has matured from an exclusive and highly specialized method for superresolution imaging of a limited set of suitable sample types, to a widespread, affordable, general purpose mode of fluorescence microscopy. STED microscopy has been expanded step by step, meeting biologist's demands of multi-color, live cell and even video rate imaging capabilities. To demonstrate this development, a number of examples are given below, although the list is by no means meant to be exhaustive.

5.1. Structural Analyses by Means of STED Microscopy

From the onset, STED microscopy has opened up a field of application for fluorescence microscopy that had previously been an exclusive domain of electron microscopy: The analysis of protein structure and distribution on the sub-organelle level. In proof-of-principle studies, cytoskeletal filaments are most often used as a standard to demonstrate superresolution (Figure 5). Neurofilaments, actin and, most frequently, tubulin are routinely imaged for comparisons of confocal and STED resolving power.[43,50,74]

In early endosomes of PC12 cells, synaptophysin and several SNARE proteins form microdomains unresolvable by conventional light microscopy but easily distinguishable in a STED setup using a pulsed far-red depletion laser.[99] The same system, achieving a lateral resolution of about 70–90 nm, has been used to show that SNAP25 forms clusters independently of the functionality of its SNARE motif, and binds to clustered syntaxin.[100] Furthermore, it was used to analyze the highly irregular fine structure of the bacterial tubulin homolog FtsZ at the early stage of cell division.[101] Structural studies of complex organelles like mitochondria also benefit from superresolution light microscopy. The mitochondrial proteins Tom20, VDAC1 and Cox2 were found to be distributed as nanoscale clusters, using custom-made STED microscopes with a lateral resolution below 50 nm.[102,103] Employing an isoSTED system, even the

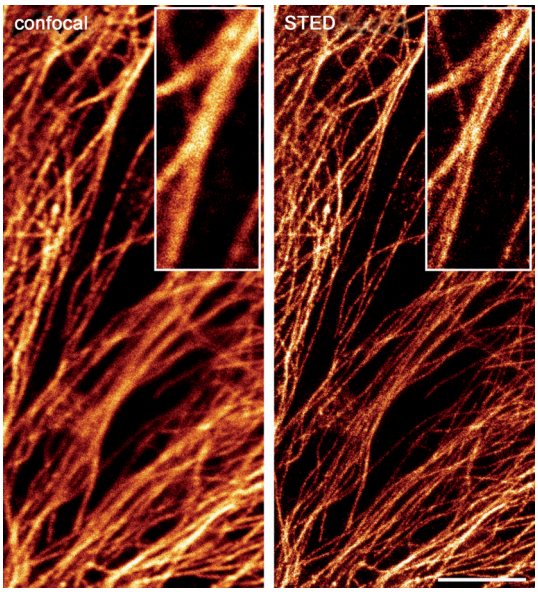

Figure 5. Microtubules of a Caco-2 cell stained with Atto647N. Comparison of confocal mode (left) and STED mode (right) at about 80 nm lateral resolution. Some large, ill-defined structures from the confocal recording emerge as bundles of multiple filaments after the depletion laser is turned on. Scale bar: 5 μm.

highly convoluted arrangement of mitochondrial cristae could be imaged with 30 nm 3D resolution.[15,47] On small vesicles with sub-diffraction diameters, superresolution can be used for size determination. For example, synaptotagmin was shown to remain clustered upon exocytosis from synaptic vesicles of primary neuronal cells.[104] STED microscopy has also been used successfully for the in vitro study of single YOYO-labeled λ-bacteriophage DNA molecules[105] and of DNA binding proteins located in human replication foci.[106]

5.2. Correlative Methods

STED and other high-resolution methods do not necessarily compete with each other. The resolution of electron or atomic force microscopy, still being superior to even the most advanced STED systems, cannot be denied. But in combination with superresolution light microscopy, these methods can be complemented by the inherent advantages of fluorescent labeling and detection. Sharma et al. combined STED visualization of the actin cytoskeleton of human ovarian cancer cells with an atomic force microscopy (AFM) based detection of changes in cell stiffness, as induced by cisplatin treatment.[107] Transmission electron microscopy (TEM), on the other hand, can be used to provide a highly detailed visualization of membrane boundaries, to which fluorescently labeled protein distributions from correlative STED images can be mapped.[108]

5.3. Multicolor STED Microscopy

However useful STED resolution power has been proven to be for structural analyses, studying protein interactions or structural-functional dependencies requires the recording of at least two separate channels. The significant differences of confocal and STED PSFs in size and sometimes shape present a severe limit for colocalization studies where these techniques are combined. Apart from special techniques like fluorescence resonance energy transfer (FRET)[109] or image correlation methods,[110] the most direct way to apply superresolution to questions of molecule interactions is multicolor STED microscopy.

Using dedicated beam pairs for the individual excitation and depletion of two fluorescent dyes, colocalization imaging of synaptic and mitochondrial protein clusters at STED resolution was demonstrated with a precision of 5 nm.[57] With the use of a supercontinuum fiber laser source, the same technique revealed colocalization patterns of various mitochondrial porins with hexokinase-1 in human U2OS cells to be much more complex than previously anticipated by confocal microscopy.[62] Different populations of synaptic vesicle proteins have also been studied by STED multiplexing and appeared not to intermix or escape from synaptic boutons upon moderate stimulation.[111,112] In whole-mount preparations of mouse cochlear inner hair cells, two-color STED microscopy was also used to investigate the colocalization of synaptotagmin 1 and the vesicular protein Vglut3.[113] By combining two-color microscopy with multi-lifetime imaging, even three channel STED microscopy has been shown to be feasible.[74]

High-resolution microscopy has undoubtedly cast a sharper light on the heterogeneities of protein distribution. However, as microscopic resolution is now of the same scale as protein clusters or even large individual proteins, colocalization coefficients can be found to be much smaller than in confocal studies, even when the two targets of interest actually interact.[114] Since the concept of colocalization is deeply tied to a finite resolution, colocalization as a tool to investigate protein interactions has been suggested to be augmented by nearest-neighbor analyses to study the spatial relations of interacting molecules.

5.4. Live-Cell STED Microscopy

Early on, STED microscopy has been explored for its capability to work with living cells.[35] For a long time, this was limited to the labeling of the plasma membrane using organic dyes or antibodies, as well as structures derived from the plasma membrane such as vesicles, after internalization of these fluorescent reporters. In hippocampal cultured neurons, live-cell STED microscopy revealed that endosomal sorting of synaptotagmin occurs rapidly, primarily involving the readily releasable pool of vesicles.[111]

Combining STED microscopy with fluorescence correlation spectroscopy (FCS), fluorescently labeled sphingolipids were shown to be transiently trapped in cholesterol-mediated molecular complexes.[67] Also by STED-FCS analysis, subtle differences in the diffusion characteristics of various fluorescent phosphoglycerolipids and their dependence on cholesterol and actin polymerization could be elucidated in such detail as remains unobtainable by standard, diffraction-limited FCS.[115]

However, only fluorescent proteins, which can be expressed in a site-specific manner fused to target proteins, provide the

versatility to visualize almost any organelle or protein distribution in a living cell. This feature has been implemented for STED microscopy only recently. After the principle had been proven,[82] the method was shown to work at 50 nm lateral resolution within live mammalian cells expressing Citrine-tubulin.[83] Using fluorescent proteins, STED microscopy has not only been used to detect structures of mammalian cells, but also for the first time to visualize the clustering of YFP tagged PIN proteins in the plasma membrane of living plant cells.[116]

Using self-labeling proteins and thus site-directed targeting of organic fluorophores, STED microscopy on living cells was further extended.[92] In a proof of principle, a lateral resolution of 40 nm was achieved, recording 10 consecutive 20 μm × 20 μm image slices with an acquisition time of 10 seconds per frame. Recently, using a STED microscope with a pulsed far-red depletion laser, $SNAP_f$-tag and $CLIP_f$-tag expression were combined successfully for multicolor live-cell STED microscopy, observing epidermal growth factor and its receptor in human embryonic kidney cells. By this approach, a lateral resolution of 80 nm was achieved.[93] With the same type of microscope, the actin cytoskeleton of living HeLa cells expressing a fluorogen-activating protein was imaged, resulting in a lateral resolution of 110 nm.[96] For STED-based studies of protein colocalization focusing on the colocalization distribution, a bimolecular fluorescence complementation technique (BiFC) has proven useful. In this system, the fluorescence of two protein fragments is reconstituted upon contact and was used in a study of tubulin interaction with the microtubule-associated protein MAP2 in living kidney epithelial cells.[117]

GFP, the most commonly used fluorescent protein, has been imaged by STED microscopy at live conditions in the plasma membrane of yeast, the endoplasmic reticulum of Vero cells and even in serotonergic neurons of the nematode *C. elegans*.[118] Even the dendritic spines of living mural hippocampal brain slices have been imaged with STED microscopy recently: first in proximity to the cover slip,[119] and later penetrating up to 90 μm into the living tissue, at 60 nm lateral resolution.[56] To this end, the correction collar of a 1.3 NA glycerol immersion objective lens had to be adjusted individually for each image slice.

5.5. STED at Video Rate

Many biological processes such as vesicle sorting occur at time scales long considered to be far below the time resolution limits of optical nanoscopy. Superresolution requires small pixel sizes and thus longer acquisition times for a given field of view. However, the focal spot size, being dependent on the intensity of the depletion laser, can be tuned, trading off spatial resolution for imaging speed. Also, speed can be increased by reducing the field of view. Thus, a compromise between resolution, speed and field of view can be found for each specific imaging task.

Labeling the surface vesicle pool of living hippocampal neurons, Westphal et al. recorded a 2.5 μm × 1.8 μm field of view at 28 frames per second (fps) and a focal spot size of 62 nm.[37] Using a suspension of nanoscale fluorescent beads, even 80 fps were reached.[120] A comparative work on STED and confocal video-rate microscopy showed nanoscopic resolution to be essential when studying synaptic vesicle transport within axons of living cultured neurons.[121] These experiments also introduced continuous-wave excitation and depletion (CW STED) into video-rate nanoscopy, benefiting from continuous photon emission as opposed to pulsed excitation, thus increasing the photon count per time frame.

6. Nanomaterials and Nanoscopy: Particle–Cell Interactions on the Nanoscale

As the building blocks of living cells are themselves nanoscale objects, applying superresolution microscopy to this field of research intuitively makes sense. However, the material sciences have advanced into the nanometer range as well, producing synthetic particles of nanometer proportions. Studying these particles and their interactions with equally small cellular components brings up the same problems and demands faced by cell biologists before, and it benefits from the same answer, namely the breaking of the diffraction limit in fluorescence microscopy.

Nanoscale materials have continually gained importance over the last years. Nanoscale particles are used for cosmetics, food production[122] and in biomedical applications, where they act as contrast agents[123–125] or as carriers or site-specific vectors for drugs and toxins. Multifunctional particles present the potential for simultaneous targeting, labeling,[126] and drug delivery, for example to cancer cells.[127] Metallic particles might even be used directly to combat cancer cells via photothermal treatment.[128,129] In addition to the intended use of nanomaterials in the biomedical field, preparation, processing and application procedures of nanoproducts[130–132] can potentially result in unintended or accidental exposure, primarily via inhalation or ingestion.[133] The small size of the nanoparticles might not only enhance their mobility inside the body, but might also allow them to enter cellular import mechanisms that remain inaccessible for materials of the same composition, but larger diameters.[134]Also, the specific mechanisms of interaction with cellular components seem to depend significantly on size, shape, composition and surface properties of the particles.[135–141] After endocytosis, particles of various designs have different destinations. They can interact with specific or random targets which might result in intracellular protein aggregation,[142] inflammatory responses[143–145] or cytotoxic effects.[146] In addition, interactions also depend on the cell type[147] as well as its metabolic state.[148]

For questions of safety and regulation, researching nanoparticle uptake, aggregation behavior and intracellular interactions and transport is therefore of great importance. Of course, nanoparticles of any size can be detected and located with respect to sub-cellular compartments at high resolution with electron microscopy.[149,150] However, nanomaterials composed of elements with a low atomic weight provide a rather poor contrast and are difficult to detect nonambiguously within the organic matrix of a cell.[151,152] With light microscopy, on the other hand, individual nanoparticles can be imaged, but dis-

cerning them from medium-sized aggregates is rather difficult. With the advent of optical farfield nanoscopy, however, this has changed.

For fluorescence microscopy, nanoparticles have to either exhibit intrinsic fluorescent properties or contain fluorescent labels. Semiconductor quantum dots are frequently used as labels for confocal or fluorescence microscopy.[153] Their extremely sharp emission peaks and their excellent photostability make them ideal candidates for multicolor cellular imaging and in vivo renal clearance studies.[153–156] However, for the time being, particles labeled with fluorescent dyes are still the most versatile tool for STED-based studies of nanoparticle-cell interactions. In the form of fluorescent beads, such particles are used routinely as a measure of STED resolving power. These are frequently commercial polystyrene or latex particles, but also silica nanoparticles with a fluorescent core have been used for STED microscopy early on.[72] With confocal microscopy, adjoining particles of sub-diffraction diameters cannot be resolved. STED microscopy, on the other hand, has allowed detailed studies of the self-assembly of nanoparticles with a diameter of 132 nm, containing a 68 nm core.[72] Investigating nanoparticle agglomeration behavior at superresolution, (Figure 6) we have found silica particles of 128 nm diameter, labeled with the Atto 647N dye, to be imported into A549 cells -a model for lung epithelial cells- within membrane-bound vesicles as single particles. Over the course of days, the particles inside the cells formed agglomerates of continually growing diameters.[157]

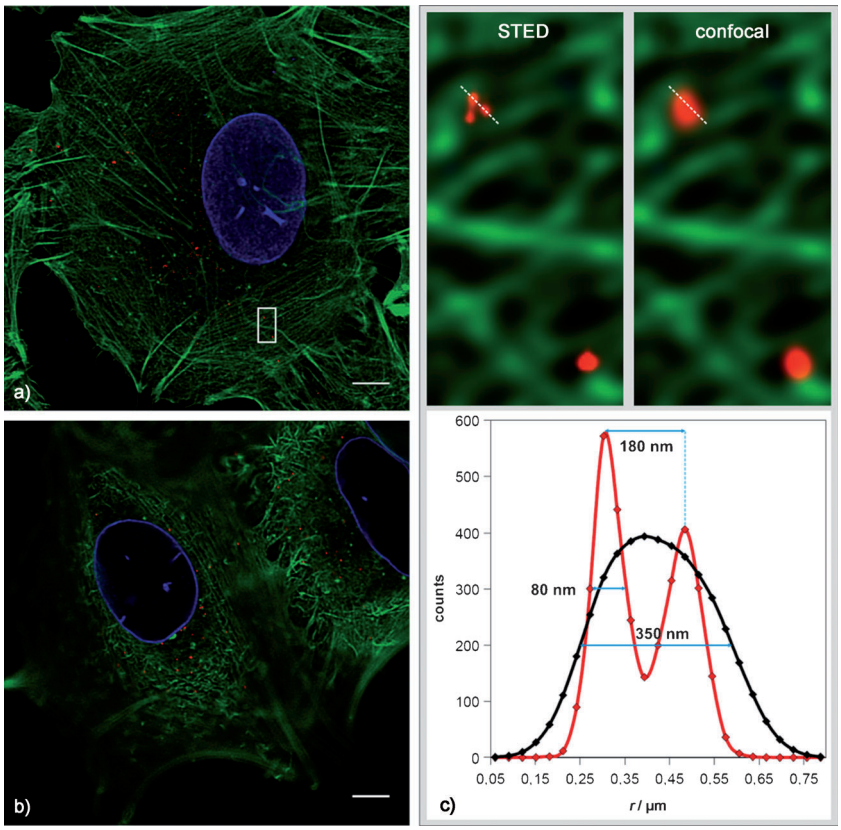

Figure 6. A549 cells after 48 h exposure to 80 nm silica particles. The particles have been internalized and have started to migrate towards the nucleus. The cell in a) is imaged close to the coverslip, in b) a more apical plane of another cell is shown. The enlarged comparison between confocal and STED recording as seen in c) corresponds to the rectangle in a). The line profiles show a distance of 180 nm between two of the three clustered particles, which is below the limit of confocal resolution. The full width at half maximum of 80 nm gives an estimate of the lateral resolution in the STED image. Green: actin stained with Alexa 488, blue: lamin B stained with Alexa 546 (both confocal), red: 80 nm silica particles fully labeled with Atto647N (STED). Scale bar: 5 µm. Images were deconvolved with Huygens software (Scientific Volume Imaging, Hilversum, Netherlands) using a classic maximum likelihood estimation algorithm.

As cellular reactions are often associated with specific subcellular compartments, it is also important to study the transport of particles and pinpoint their final destination within the cell with high accuracy. This can help in understanding which mechanisms allow particles of different size, shape and composition to cross the plasma membrane, get distributed within the cell and reach destinations such as lysosomes, mitochondria or the cell nucleus.[142,158–161] Employing STED microscopy with a pulsed Ti:Sapphire depletion laser, we have studied the uptake and destinations of silica nanospheres in Caco-2 cells, derived from the human intestine.[162] Particles of 83 nm and 32 nm, respectively, were shown to migrate towards a juxtanuclear pool over a period of several days, without colocalizing with the lysosome marker LAMP1. Only 32 nm particles were eventually detected inside the nucleus, implicating a size-selective transport. Larger aggregates did occur inside the nucleus, but only after several days of exposure, indicating that agglomeration occurred after nuclear import. Size-selectivity is a known property of nuclear pores,[163,164] which leads us to suggest that silica nanoparticles below a certain diameter can enter the nucleus of Caco-2 cells via nuclear pore complexes.

This shows that superresolution microscopy can be used to localize single particles with high accuracy, even at the sub-organelle level. Together with studying interactions of nanoparticles with specific proteins of interest, this can help answering the question if and how nanoparticles affect living cells, and ultimately provide clues as to how particle properties might be adapted to enhance biocompatibility.

7. Summary and Outlook

Light microscopy is and has always been a matter of compromise. A number of systems and principles coexist, all of them

offering a unique set of advantages and disadvantages, leaving the end user to decide which fits best to the tasks at hand and to the demands of the respective line of research. Superresolution light microscopy is a new addition to the methodological palette, introducing several techniques and working principles competing with each other.

The technique of STED microscopy is still evolving. At the same time, it is the one fluorescence-based superresolution method that has reached a degree of versatility to make it ready for routine use not only by specialists in experimental physics, but also by the end user in the material or life sciences. Here, it shows great promise to lead to a deeper, more detailed understanding of processes that could previously only be studied either at low resolution or under highly artificial conditions. For some topics of research such as interactions of nanoparticles with cells, the introduction of optical superresolution not simply means an increase in performance, but marks a turning point where light microscopy becomes a truly useful tool for standard use. Here the technique can be expected to provide much insight in the near future.

A number of important milestones have been reached and implemented into the basic principle of STED microscopy in the last few years, namely spectral multiplexing, life-cell and video-rate imaging and the development of technical upgrades like CW STED, the vortex phase plate or time gating, thereby continuously improving the method's performance. At the same time, accessory instruments such as detectors keep pace with these developments, becoming faster and more sensitive. The same is true for advanced labeling systems which allow pushing the method towards its true limits regarding resolution, live-cell capabilities and prolonged time-lapse imaging. The comparatively wide range of suitable fluorophores, among them organic molecules as well as fluorescent proteins, further increases the versatility of the method. A unique feature of STED among the superresolution techniques is its ability to be combined with spectroscopic methods beyond pure imaging.

However, it is not the end of the road yet. Other methods such as the various pointillistic types of microscopy have emerged and have recently gained some ground by commercial implementation. They excel at lateral resolution enhancement but are hampered in other ways. In many cases the palette of suitable fluorophores is limited to switchable fluorescent dyes; in others the imaging speed is far too slow for live-cell applications or the imaging depth is insufficient. As with STED microscopy, much effort is put into further developing these techniques and in overcoming their limits. Today, the question is not so much if superresolution microscopy will one day be user-friendly, powerful and versatile enough to become a routine tool for investigations in the nanometer range, but which method is the right one for the biological question to be answered. Personally, these authors are already looking forward to multicolor video-rate STED microscopy with isotropic 3D resolution of a few ten nanometers.

Acknowledgements

The authors acknowledge the financial support of the German Federal Ministry of Education and Research (BMBF) for this work, within the project "Mechanismen der Nanotoxizität durch modernste mikroskopische Methoden, MeNatox, Förderkennzeichen: 03X0063". We thank Eduard Arzt for continuing support of our work at INM. We also thank Marius Weber for excellent assistance with the bibliographic data and Katharina Narr for proofreading the manuscript. We thank Christian Cavelius and Sarah Schmidt for providing labeled silica particles and Katharina Narr and Melanie Kucki for providing A549 and Caco-2 cells.

Keywords: dual-color imaging · fluorescence · live-cell imaging · nanoparticles · superresolution microscopy

[1] C. A. Combs, *Curr. Prot. Neurosci.* **2010**, *50,* 2.1.1-2.1.14.
[2] K. M. Marks, G. P. Nolan, *Nat. Methods* **2006**, *3*, 591 – 596.
[3] J. T. Wessels, K. Yamauchi, R. M. Hoffman, F. S. Wouters, *Cytometry Part A* **2010**, *77*, 667 – 676.
[4] T. Zimmermann, J. Rietdorf, R. Pepperkok, *FEBS Lett.* **2003**, *546*, 87 – 92.
[5] H. Tsurui, H. Nishimura, S. Hattori, S. Hirose, K. Okumura, T. Shirai, *J. Histochem. Cytochem.* **2000**, *48*, 653 – 682.
[6] J. D. Brain, M. A. Curran, T. Donaghey, R. M. Molina, *Nanotoxicology* **2009**, *3*, 174 – 180.
[7] K. Unfried, C. Albrecht, L. O. Klotz, A. von Mikecz, S. Grether-Beck, R. P. F. Schins, *Nanotoxicology* **2007**, *1*, 52 – 71.
[8] R. Tantra, A. Knight, *Nanotoxicology* **2011**, *5*, 381 – 392.
[9] J. B. Pawley, *Handbook of Biological Confocal Microscopy*, Springer, Berlin, **2006**.
[10] T. Wilson, C. Sheppard, *Theory and Practice of Scanning Optical Microscopy*, Academic Press, London, **1984**.
[11] P. I. H. Bastiaens, A. Squire, *Trends Cell Biol.* **1999**, *9*, 48 – 51.
[12] I. I. Smalyukh, S. V. Shiyanovskii, O. D. Lavrentovich, *Chem. Phys. Lett.* **2001**, *336*, 88 – 96.
[13] R. Rigler, Ü. Mets, J. Widengren, P. Kask, *Eur. Biophys. J.* **1993**, *22*, 169 – 175.
[14] H. Qian, E. L. Elson, *Appl. Opt.* **1991**, *30*, 1185 – 1195.
[15] S. W. Hell, *Nat. Methods* **2009**, *6*, 24 – 32.
[16] E. Betzig, G. H. Patterson, R. Sougrat, O. W. Lindwasser, S. Olenych, J. S. Bonifacino, M. W. Davidson, J. Lippincott-Schwartz, H. F. Hess, *Science* **2006**, *313*, 1642 – 1645.
[17] M. J. Rust, M. Bates, X. Zhuang, *Nat. Methods* **2006**, *3*, 793 – 796.
[18] M. Heilemann, S. van de Linde, M. Schüttpelz, R. Kasper, B. Seefeldt, A. Mukherjee, P. Tinnefeld, M. Sauer, *Angew. Chem.* **2008**, *120*, 6266 – 6271; *Angew. Chem. Int. Ed.* **2008**, *47*, 6172 – 6176.
[19] A. Egner, C. Geisler, C. von Middendorff, H. Bock, D. Wenzel, R. Medda, M. Andresen, A. C. Stiel, S. Jakobs, C. Eggeling, *Biophys. J.* **2007**, *93*, 3285 – 3290.
[20] P. Lemmer, M. Gunkel, D. Baddeley, R. Kaufmann, A. Urich, Y. Weiland, J. Reymann, P. Müller, M. Hausmann, C. Cremer, *Appl. Phys. B* **2008**, *93*, 1 – 12.
[21] M. G. L. Gustafsson, *J. Microsc.* **2000**, *198*, 82 – 87.
[22] R. Heintzmann, P. A. Benedetti, *Appl. Opt.* **2006**, *45*, 5037 – 5045.
[23] M. G. L. Gustafsson, L. Shao, P. M. Carlton, C. J. R. Wang, I. N. Golubovskaya, W. Z. Cande, D. A. Agard, J. W. Sedat, *Biophys. J.* **2008**, *94*, 4957 – 4970.
[24] R. Heintzmann, T. M. Jovin, C. Cremer, *J. Opt. Soc. Am. A* **2002**, *19*, 1599 – 1609.
[25] M. G. L. Gustafsson, *Proc. Natl. Acad. Sci. USA* **2005**, *102*, 13081 – 13086.
[26] P. Bingen, M. Reuss, J. Engelhardt, S. W. Hell, *Opt. Express* **2011**, *19*, 23716 – 23726.
[27] J. Bewersdorf, R. Pick, S. W. Hell, *Opt. Lett.* **1998**, *23*, 655 – 657.
[28] S. W. Hell, E. H. K. Stelzer, S. Lindek, C. Cremer, *Opt. Lett.* **1994**, *19*, 222 – 224.
[29] S. W. Hell, *Phys. Lett. A* **2004**, *326*, 140 – 145.

[30] S. W. Hell, S. Jakobs, L. Kastrup, *Appl. Phys. A* **2003**, *77*, 859 – 860.
[31] T. Grotjohann, I. Testa, M. Leutenegger, H. Bock, N. T. Urban, F. Lavoie-Cardinal, K. I. Willig, C. Eggeling, S. Jakobs, S. W. Hell, *Nature* **2011**, *478*, 204 – 208.
[32] S. W. Hell, M. Kroug, *Appl. Phys. B* **1995**, *60*, 495 – 497.
[33] S. Bretschneider, C. Eggeling, S. W. Hell, *Phys. Rev. Lett.* **2007**, *98*, 218103.
[34] S. W. Hell, J. Wichmann, *Opt. Lett.* **1994**, *19*, 780 – 782.
[35] T. A. Klar, S. Jakobs, M. Dyba, A. Egner, S. W. Hell, *Proc. Natl. Acad. Sci. USA* **2000**, *97*, 8206 – 8210.
[36] S. W. Hell, *Science* **2007**, *316*, 1153 – 1158.
[37] V. Westphal, S. O. Rizzoli, M. A. Lauterbach, D. Kamin, R. Jahn, S. W. Hell, *Science* **2008**, *320*, 246 – 249.
[38] E. Rittweger, K. Y. Han, S. E. Irvine, C. Eggeling, S. W. Hell, *Nat. Photonics* **2009**, *3*, 144 – 147.
[39] M. Dyba, S. W. Hell, *Appl. Opt.* **2003**, *42*, 5123 – 5129.
[40] J.-I. Hotta, E. Fron, P. Dedecker, K. P. F. Janssen, C. Li, K. Müllen, B. Harke, J. Bückers, S. W. Hell, J. Hofkens, *J. Am. Chem. Soc.* **2010**, *132*, 5021 – 5023.
[41] G. Donnert, J. Keller, R. Medda, M. A. Andrei, S. O. Rizzoli, R. Lührmann, R. Jahn, C. Eggeling, S. W. Hell, *Proc. Natl. Acad. Sci. USA* **2006**, *103*, 11440 – 11445.
[42] J. Vogelsang, R. Kasper, C. Steinhauer, B. Person, M. Heilemann, M. Sauer, P. Tinnefeld, *Angew. Chem.* **2008**, *120*, 5545 – 5550; *Angew. Chem. Int. Ed.* **2008**, *47*, 5465 – 5469.
[43] R. Kasper, B. Harke, C. Forthmann, P. Tinnefeld, S. W. Hell, M. Sauer, *Small* **2010**, *6*, 1379 – 1384.
[44] P. Török, P. Munro, *Opt. Express* **2004**, *12*, 3605 – 3617.
[45] J. Keller, A. Schönle, S. W. Hell, *Opt. Express* **2007**, *15*, 3361 – 3371.
[46] M. Reuss, J. Engelhardt, S. W. Hell, *Opt. Express* **2010**, *18*, 1049 – 1058.
[47] R. Schmidt, C. A. Wurm, A. Punge, A. Egner, S. Jakobs, S. W. Hell, *Nano Lett.* **2009**, *9*, 2508 – 2510.
[48] M. Dyba, S. Hell, *Phys. Rev. Lett.* **2002**, *88*, 163901.
[49] M. Leutenegger, C. Eggeling, S. W. Hell, *Opt. Express* **2010**, *18*, 26417 – 26429.
[50] K. I. Willig, B. Harke, R. Medda, S. W. Hell, *Nat. Methods* **2007**, *4*, 915 – 918.
[51] W. Denk, J. H. Strickler, W. W. Webb, *Science* **1990**, *248*, 73 – 76.
[52] G. Moneron, S. W. Hell, *Opt. Express* **2009**, *17*, 14567 – 14573.
[53] Q. Li, S. S. H. Wu, K. C. Chou, *Biophys. J.* **2009**, *97*, 3224 – 3228.
[54] J. B. Ding, K. T. Takasaki, B. L. Sabatini, *Neuron* **2009**, *63*, 429 – 437.
[55] A. Diaspro, P. Bianchini, F. Cella-Zanacchi, B. Harke, M. Perrone, E. Ronzitti, S. Galiani, J. Chacko, Z. Lavagnino, *Microsc. Anal.* **2011**, *25*, 13 – 17.
[56] N. T. Urban, K. I. Willig, S. W. Hell, U. V. Nägerl, *Biophys. J.* **2011**, *101*, 1277 – 1284.
[57] G. Donnert, J. Keller, C. A. Wurm, S. O. Rizzoli, V. Westphal, A. Schönle, R. Jahn, S. Jakobs, C. Eggeling, S. W. Hell, *Biophys. J.* **2007**, *92*, L67 – L69.
[58] H. Blom, D. Rönnlund, L. Scott, Z. Spicarova, V. Rantanen, J. Widengren, A. Aperia, H. Brismar, *Microsc. Res. Tech.* **2012**, *75*, 220 – 228.
[59] R. Schmidt, C. A. Wurm, S. Jakobs, J. Engelhardt, A. Egner, S. W. Hell, *Nat. Methods* **2008**, *5*, 539 – 544.
[60] K. Friedemann, A. Turshatov, K. Landfester, D. Crespy, *Langmuir* **2011**, *27*, 7132 – 7139.
[61] L. Meyer, D. Wildanger, R. Medda, A. Punge, S. O. Rizzoli, G. Donnert, S. W. Hell, *Small* **2008**, *4*, 1095 – 1100.
[62] D. Neumann, J. Bückers, L. Kastrup, S. W. Hell, S. Jakobs, *PMC Biophys.* **2010**, *3*, 4.
[63] K. I. Willig, A. C. Stiel, T. Brakemann, S. Jakobs, S. W. Hell, *Nano Lett.* **2011**, *11*, 3970 – 3973.
[64] J. R. Moffitt, C. Osseforth, J. Michaelis, *Opt. Express* **2011**, *19*, 4242 – 4254.
[65] G. Vicidomini, G. Moneron, K. Y. Han, V. Westphal, H. Ta, M. Reuss, J. Engelhardt, C. Eggeling, S. W. Hell, *Nat. Methods* **2011**, *8*, 571 – 573.
[66] L. Kastrup, H. Blom, C. Eggeling, S. W. Hell, *Phys. Rev. Lett.* **2005**, *94*, 178104.
[67] C. Eggeling, C. Ringemann, R. Medda, G. Schwarzmann, K. Sandhoff, S. Polyakova, V. N. Belov, B. Hein, C. von Middendorff, A. Schönle, S. W. Hell, *Nature* **2009**, *457*, 1159 – 1162.
[68] C. Ringemann, B. Harke, C. Von Middendorff, R. Medda, A. Honigmann, R. Wagner, M. Leutenegger, A. Schönle, S. W. Hell, C. Eggeling, *New J. Phys.* **2009**, *11*, 103054.
[69] E. Auksorius, B. R. Boruah, C. Dunsby, P. M. P. Lanigan, G. Kennedy, M. A. A. Neil, P. M. W. French, *Opt. Lett.* **2008**, *33*, 113 – 115.
[70] V. Westphal, L. Kastrup, S. W. Hell, *Appl. Phys. B* **2003**, *77*, 377 – 380.
[71] J. J. Sieber, K. I. Willig, R. Heintzmann, S. W. Hell, T. Lang, *Biophys. J.* **2006**, *90*, 2843 – 2851.
[72] K. I. Willig, J. Keller, M. Bossi, S. W. Hell, *New J. Phys.* **2006**, *8*, 106 – 106.
[73] D. Wildanger, E. Rittweger, L. Kastrup, S. W. Hell, *Opt. Express* **2008**, *16*, 9614 – 9621.
[74] J. Bückers, D. Wildanger, G. Vicidomini, L. Kastrup, S. W. Hell, *Opt. Express* **2011**, *19*, 3130 – 3143.
[75] C. Kuang, W. Zhao, G. Wang, *Rev. Sci. Instrum.* **2010**, *81*, 053709.
[76] K. Kolmakov, V. N. Belov, J. Bierwagen, C. Ringemann, V. Müller, C. Eggeling, S. W. Hell, *Chem. Eur. J.* **2010**, *16*, 158 – 166.
[77] K. Kolmakov, V. N. Belov, C. A. Wurm, B. Harke, M. Leutenegger, C. Eggeling, S. W. Hell, *Eur. J. Org. Chem.* **2010**, 3593 – 3610.
[78] G. Y. Mitronova, V. N. Belov, M. L. Bossi, C. A. Wurm, L. Meyer, R. Medda, G. Moneron, S. Bretschneider, C. Eggeling, S. Jakobs, S. W. Hell, *Chem. Eur. J.* **2010**, *16*, 4477 – 4488.
[79] N. C. Shaner, P. A. Steinbach, R. Y. Tsien, *Nat. Methods* **2005**, *2*, 905 – 909.
[80] N. C. Shaner, G. H. Patterson, M. W. Davidson, *J. Cell Sci.* **2007**, *120*, 4247 – 4260.
[81] R. Y. Tsien, *Annu. Rev. Biochem.* **1998**, *67*, 509 – 544.
[82] K. I. Willig, R. R. Kellner, R. Medda, B. Hein, S. Jakobs, S. W. Hell, *Nat. Methods* **2006**, *3*, 721 – 723.
[83] B. Hein, K. I. Willig, S. W. Hell, *Proc. Natl. Acad. Sci. USA* **2008**, *105*, 14271 – 14276.
[84] U. V. Nägerl, K. I. Willig, B. Hein, S. W. Hell, T. Bonhoeffer, *Proc. Natl. Acad. Sci. USA* **2008**, *105*, 18982 – 18987.
[85] R. L. Strack, B. Hein, D. Bhattacharyya, S. W. Hell, R. J. Keenan, B. S. Glick, *Biochemistry* **2009**, *48*, 8279 – 8281.
[86] K. S. Morozova, K. D. Piatkevich, T. J. Gould, J. Zhang, J. Bewersdorf, V. V. Verkhusha, *Biophys. J.* **2010**, *99*, L13 – L15.
[87] D. Shcherbo, E. M. Merzlyak, T. V. Chepurnykh, A. F. Fradkov, G. V. Ermakova, E. A. Solovieva, K. A. Lukyanov, E. A. Bogdanova, A. G. Zaraisky, S. Lukyanov, D. M. Chudakov, *Nat. Methods* **2007**, *4*, 741 – 746.
[88] G. V. Los, L. P. Encell, M. G. McDougall, D. D. Hartzell, N. Karassina, C. Zimprich, M. G. Wood, R. Learish, R. F. Ohana, M. Urh, D. Simpson, J. Mendez, K. Zimmerman, P. Otto, G. Vidugiris, A. Darzins, D. H. Klaubert, R. F. Bulleit, K. V. Wood, *ACS Chem. Biol.* **2008**, *3*, 373 – 382.
[89] J. Schröder, H. Benink, M. Dyba, G. V. Los, *Biophys. J.* **2009**, *96*, L1 – L3.
[90] A. Keppler, S. Gendreizig, T. Gronemeyer, H. Pick, H. Vogel, K. Johnsson, *Nat. Biotechnol.* **2003**, *21*, 86 – 89.
[91] A. Gautier, A. Juillerat, C. Heinis, I. R. Corrêa, M. Kindermann, F. Beaufils, K. Johnsson, *Chem. Biol.* **2008**, *15*, 128 – 136.
[92] B. Hein, K. I. Willig, C. A. Wurm, V. Westphal, S. Jakobs, S. W. Hell, *Biophys. J.* **2010**, *98*, 158 – 163.
[93] P. A. Pellett, X. Sun, T. J. Gould, J. E. Rothman, M.-Q. Xu, I. R. Corrêa, J. Bewersdorf, *Biomed. Opt. Express* **2011**, *2*, 2364 – 2371.
[94] X. Sun, A. Zhang, B. Baker, L. Sun, A. Howard, J. Buswell, D. Maurel, A. Masharina, K. Johnsson, C. J. Noren, M.-Q. Xu, I. R. Corrêa, *ChemBioChem* **2011**, *12*, 2217 – 2226.
[95] C. Szent-Gyorgyi, B. A. Schmidt, Y. Creeger, G. W. Fisher, K. L. Zakel, S. Adler, J. A. J. Fitzpatrick, C. A. Woolford, Q. Yan, K. V. Vasilev, P. B. Berget, M. P. Bruchez, J. W. Jarvik, A. Waggoner, *Nat. Biotechnol.* **2008**, *26*, 235 – 240.
[96] J. A. J. Fitzpatrick, Q. Yan, J. J. Sieber, M. Dyba, U. Schwarz, C. Szent-Gyorgyi, C. A. Woolford, P. B. Berget, A. S. Waggoner, M. P. Bruchez, *Bioconjugate Chem.* **2009**, *20*, 1843 – 1847.
[97] S. E. Irvine, T. Staudt, E. Rittweger, J. Engelhardt, S. W. Hell, *Angew. Chem.* **2008**, *120*, 2725 – 2728; *Angew. Chem. Int. Ed.* **2008**, *47*, 2685 – 2688.
[98] Y. K. Tzeng, O. Faklaris, B. M. Chang, Y. Kuo, J. H. Hsu, H. C. Chang, *Angew. Chem.* **2011**, *123*, 2310 – 2313; *Angew. Chem. Int. Ed.* **2011**, *50*, 2262 – 2265.
[99] U. Geumann, C. Schäfer, D. Riedel, R. Jahn, S. O. Rizzoli, *Microsc. Res. Tech.* **2010**, *73*, 606 – 617.

[100] N. D. Halemani, I. Bethani, S. O. Rizzoli, T. Lang, *Traffic* **2010**, *11*, 394 – 404.
[101] P. C. Jennings, G. C. Cox, L. G. Monahan, E. J. Harry, *Micron* **2011**, *42*, 336 – 341.
[102] H. Singh, R. Lu, P. F. G. Rodríguez, Y. Wu, J. C. Bopassa, E. Stefani, L. Toro, *Mitochondrion* **2011**, DOI: 10.1016/j.mito.2011.09.004.
[103] C. A. Wurm, D. Neumann, R. Schmidt, A. Egner, S. Jakobs, *Meth. Mol. Biol.* **2010**, *591*, 185 – 199.
[104] K. I. Willig, S. O. Rizzoli, V. Westphal, R. Jahn, S. W. Hell, *Nature* **2006**, *440*, 935 – 939.
[105] F. Persson, P. Bingen, T. Staudt, J. Engelhardt, J. O. Tegenfeldt, S. W. Hell, *Angew. Chem.* **2011**, *123*, 5696 – 5698; *Angew. Chem. Int. Ed.* **2011**, *50*, 5581 – 5583.
[106] Z. Cseresnyes, U. Schwarz, C. M. Green, *BMC Cell Biol.* **2009**, *10*, 88.
[107] S. Sharma, C. Santiskulvong, L. Bentolila, J. Rao, O. Dorigo, J. K. Gimzewski, *Nanomedicine: Nanotechnology, Biology and Medicine* **2011**, DOI: 10.1016/j.nano.2011.09.015.
[108] S. Watanabe, A. Punge, G. Hollopeter, K. I. Willig, R. J. Hobson, M. W. Davis, S. W. Hell, E. M. Jorgensen, *Nat. Methods* **2011**, *8*, 80 – 84.
[109] L. Stryer, *Annu. Rev. Biochem.* **1978**, *47*, 819 – 846.
[110] M. A. Digman, E. Gratton, *Annu. Rev. Phys. Chem.* **2011**, *62*, 645 – 668.
[111] P. Hoopmann, A. Punge, S. V. Barysch, V. Westphal, J. Buckers, F. Opazo, I. Bethani, M. A. Lauterbach, S. W. Hell, S. O. Rizzoli, *Proc. Natl. Acad. Sci. USA* **2010**, *107*, 19055 – 19060.
[112] F. Opazo, A. Punge, J. Bückers, P. Hoopmann, L. Kastrup, S. W. Hell, S. O. Rizzoli, *Traffic* **2010**, *11*, 800 – 812.
[113] E. Reisinger, C. Bresee, J. Neef, R. Nair, K. Reuter, A. Bulankina, R. Nouvian, M. Koch, J. Buckers, L. Kastrup, I. Roux, C. Petit, S. W. Hell, N. Brose, J. S. Rhee, S. Kugler, J. V. Brigande, T. Moser, *J. Neurosci.* **2011**, *31*, 4886 – 4895.
[114] H. Blom, D. Rönnlund, L. Scott, Z. Spicarova, J. Widengren, A. Bondar, A. Aperia, H. Brismar, *BMC Neurosci.* **2011**, *12*, 16.
[115] V. Mueller, C. Ringemann, A. Honigmann, G. Schwarzmann, R. Medda, M. Leutenegger, S. Polyakova, V. N. Belov, S. W. Hell, C. Eggeling, *Biophys. J.* **2011**, *101*, 1651 – 1660.
[116] J. Kleine-Vehn, K. Wabnik, A. Martinière, Ł. Łangowski, K. Willig, S. Naramoto, J. Leitner, H. Tanaka, S. Jakobs, S. Robert, C. Luschnig, W. Govaerts, S. W. Hell, J. Runions, J. Friml, *Mol. Syst. Biol.* **2011**, *7*.
[117] B. Lalkens, I. Testa, K. I. Willig, S. W. Hell, *Microsc. Res. Tech.* **2012**, *75*, 1 – 6.
[118] B. R. Rankin, G. Moneron, C. A. Wurm, J. C. Nelson, A. Walter, D. Schwarzer, J. Schroeder, D. A. Colón-Ramos, S. W. Hell, *Biophys. J.* **2011**, *100*, L63 – L65.
[119] U. V. Nägerl, T. Bonhoeffer, *J. Neurosci.* **2010**, *30*, 9341 – 9346.
[120] V. Westphal, M. A. Lauterbach, A. Di Nicola, S. W. Hell, *New J. Phys.* **2007**, *9*, 435 – 435.
[121] M. A. Lauterbach, J. Keller, A. Schönle, D. Kamin, V. Westphal, S. O. Rizzoli, S. W. Hell, *J. Biophotonics* **2010**, *3*, 417 – 424.
[122] S. Dekkers, P. Krystek, R. J. B. Peters, D. P. K. Lankveld, B. G. H. Bokkers, P. H. van Hoeven-Arentzen, H. Bouwmeester, A. G. Oomen, *Nanotoxicology* **2011**, *5*, 393 – 405.
[123] A. W. H. Lin, N. A. Lewinski, J. L. West, N. J. Halas, R. A. Drezek, *J. Biomed. Opt.* **2005**, *10*, 064035.
[124] J. F. Hainfeld, *Br. J. Radiol.* **2006**, *79*, 248 – 253.
[125] Y. Jin, C. Jia, S.-W. Huang, M. O'Donnell, X. Gao, *Nat. Commun.* **2010**, *1*, 1 – 8.
[126] X.-X. Meng, J.-Q. Wan, M. Jing, S.-G. Zhao, W. Cai, E.-Z. Liu, *Acta Pharmacol. Sin.* **2007**, *28*, 2019 – 2026.
[127] M. Das, D. Mishra, P. Dhak, S. Gupta, T. K. Maiti, A. Basak, P. Pramanik, *Small* **2009**, *5*, 2883 – 2893.
[128] T. B. Huff, L. Tong, Y. Zhao, M. N. Hansen, J. X. Cheng, A. Wei, *Nanomedicine* **2007**, *2*, 125 – 132.
[129] C. S. Rejiya, J. Kumar, V. Raji, M. Vibin, A. Abraham, *Pharmacol. Res.* **2012**, *65*, 261 – 269
[130] O. W. Flörke, *Ullmann's Encyclopedia of Industrial Chemistry*, Wiley-VCH, Weinheim. **2007**, pp. 1 – 89.
[131] *Nanoscience and Nanotechnologies: Opportunities and Uncertainties*, The Royal Society, London, **2004**.
[132] nano.DE-Report: Status quo der Nanotechnologie in Deutschland Bundesministerium für Bildung und Forschung BMBF Bonn, Berlin, **2011**.
[133] G. Oberdörster, E. Oberdörster, J. Oberdörster, *Environ. Health Perspect.* **2005**, *113*, 823 – 839.
[134] G. Oberdörster, *J. Intern. Med.* **2010**, *267*, 89 – 105.
[135] L. Gonzalez, L. C. J. Thomassen, G. Plas, V. Rabolli, D. Napierska, I. Decordier, M. Roelants, P. H. Hoet, C. E. A. Kirschhock, J. A. Martens, D. Lison, M. Kirsch-Volders, *Nanotoxicology* **2010**, *4*, 382 – 395.
[136] V. Rabolli, L. C. J. Thomassen, C. Princen, D. Napierska, L. Gonzalez, M. Kirsch-Volders, P. H. Hoet, F. Huaux, C. E. A. Kirschhock, J. A. Martens, D. Lison, *Nanotoxicology* **2010**, *4*, 307 – 318.
[137] J. Rejman, V. Oberle, I. S. Zuhorn, D. Hoekstra, *Biochem. J.* **2004**, *377*, 159 – 169.
[138] M. J. D. Clift, B. Rothen-Rutishauser, D. M. Brown, R. Duffin, K. Donaldson, L. Proudfoot, K. Guy, V. Stone, *Toxicol. Appl. Pharmacol.* **2008**, *232*, 418 – 427.
[139] X. Huang, X. Teng, D. Chen, F. Tang, J. He, *Biomaterials* **2010**, *31*, 438 – 448.
[140] H. F. Krug, P. Wick, *Angew. Chem.* **2011**, *123*, 1294 – 1314; *Angew. Chem. Int. Ed.* **2011**, *50*, 1260 – 1278.
[141] A. E. Nel, L. Mädler, D. Velegol, T. Xia, E. M. V. Hoek, P. Somasundaran, F. Klaessig, V. Castranova, M. Thompson, *Nat. Mater.* **2009**, *8*, 543 – 557.
[142] M. Chen, A. von Mikecz, *Exp. Cell Res.* **2005**, *305*, 51 – 62.
[143] M. Singal, J. N. Finkelstein, *Exp. Lung Res.* **2005**, *31*, 581 – 597.
[144] S. C. Brown, M. Kamal, N. Nasreen, A. Baumuratov, P. Sharma, V. B. Antony, B. M. Moudgil, *Adv. Powder Technol.* **2007**, *18*, 69 – 79.
[145] T. Xia, M. Kovochich, J. Brant, M. Hotze, J. Sempf, T. Oberley, C. Sioutas, J. I. Yeh, M. R. Wiesner, A. E. Nel, *Nano Lett.* **2006**, *6*, 1794 – 1807.
[146] Z. M. Tao, E. Jones, J. Goodisman, A. K. Souid, *Anal. Biochem.* **2008**, *381*, 43 – 52.
[147] C. A. Barnes, A. Elsaesser, J. Arkusz, A. Smok, J. Palus, A. Lesniak, A. Salvati, J. P. Hanrahan, W. H. De Jong, E. Dziubaltowska, M. Stepnik, K. Rydzynski, G. McKerr, I. Lynch, K. A. Dawson, C. V. Howard, *Nano Lett.* **2008**, *8*, 3069 – 3074.
[148] J.-S. Chang, K. L. B. Chang, H. Deng-Fwu, Z.-L. Kong, *Environ. Sci. Technol.* **2007**, *41*, 2064 – 2068.
[149] M. V. D. Z. Park, H. W. Verharen, E. Zwart, L. G. Hernandez, J. van Benthem, A. Elsaesser, C. Barnes, G. McKerr, C. V. Howard, A. Salvati, I. Lynch, K. A. Dawson, W. H. de Jong, *Nanotoxicology* **2011**, *5*, 168 – 181.
[150] Y. Qiu, Y. Liu, L. Wang, L. Xu, R. Bai, Y. Ji, X. Wu, Y. Zhao, Y. Li, C. Chen, *Biomaterials* **2010**, *31*, 7606 – 7619.
[151] C. Mühlfeld, B. Rothen-Rutishauser, D. Vanhecke, F. Blank, P. Gehr, M. Ochs, *Part. Fibre Toxicol.* **2007**, *4*, 11.
[152] C. Brandenberger, M. J. D. Clift, D. Vanhecke, C. Mühlfeld, V. Stone, P. Gehr, B. Rothen-Rutishauser, *Part. Fibre Toxicol.* **2010**, *7*, 15.
[153] A. P. Alivisatos, W. Gu, C. Larabell, *Annu. Rev. Biomed. Eng.* **2005**, *7*, 55 – 76.
[154] H. Soo Choi, W. Liu, P. Misra, E. Tanaka, J. P. Zimmer, B. Itty Ipe, M. G. Bawendi, J. V. Frangioni, *Nat. Biotechnol.* **2007**, *25*, 1165 – 1170.
[155] U. Resch-Genger, M. Grabolle, S. Cavaliere-Jaricot, R. Nitschke, T. Nann, *Nat. Methods* **2008**, *5*, 763 – 775.
[156] M. J. D. Clift, C. Brandenberger, B. Rothen-Rutishauser, D. M. Brown, V. Stone, *Toxicology* **2011**, *286*, 58 – 68.
[157] S. Schübbe, C. Cavelius, C. Schumann, M. Koch, A. Kraegeloh, *Adv. Eng. Mater.* **2010**, *12*, 417 – 422.
[158] C. Brandenberger, C. Mühlfeld, Z. Ali, A.-G. Lenz, O. Schmid, W. J. Parak, P. Gehr, B. Rothen-Rutishauser, *Small* **2010**, *6*, 1669 – 1678.
[159] A. M. Derfus, W. C. W. Chan, S. N. Bhatia, *Adv. Mater.* **2004**, *16*, 961 – 966.
[160] G. Ruan, A. Agrawai, A. I. Marcus, S. Nie, *J. Am. Chem. Soc.* **2007**, *129*, 14759 – 14766.
[161] L. W. Zhang, N. A. Monteiro-Riviere, *Toxicol. Sci.* **2009**, *110*, 138 – 155.
[162] S. Schübbe, C. Schumann, C. Cavelius, M. Koch, T. Müller, A. Kraegeloh, *Chem. Mater.* **2011**, DOI: 10.1021/cm2018532, 1 – 10.
[163] M. Beck, F. Förster, M. Ecke, J. M. Plitzko, F. Melchior, G. Gerisch, W. Baumeister, O. Medalia, *Science* **2004**, *306*, 1387 – 1390.
[164] N. Panté, M. Kann, *Mol. Biol. Cell* **2002**, *13*, 425 – 434.
[165] V. N. Belov, C. A. Wurm, V. P. Boyarskiy, S. Jakobs, S. W. Hell, *Angew. Chem.* **2010**, *122*, 3598 – 3602; *Angew. Chem. Int. Ed.* **2010**, *49*, 3520 – 3523.
[166] S. M. Polyakova, V. N. Belov, S. F. Yan, C. Eggeling, C. Ringemann, G. Schwarzmann, A. de Meijere, S. W. Hell, *Eur. J. Org. Chem.* **2009**, *30*, 5162 – 5177.

[167] D. Wildanger, R. Medda, L. Kastrup, S. W. Hell, *J. Microsc.* **2009**, *236*, 35 – 43.
[168] G. Moneron, R. Medda, B. Hein, A. Giske, V. Westphal, S. W. Hell, *Opt. Express* **2010**, *18*, 1302 – 1309.
[169] B. R. Rankin, R. R. Kellner, S. W. Hell, *Opt. Lett.* **2008**, *33*, 2491 – 2493.
[170] D. Fitzner, A. Schneider, A. Kippert, W. Möbius, K. I. Willig, S. W. Hell, G. Bunt, K. Gaus, M. Simons, *EMBO J.* **2006**, *25*, 5037 – 5048.
[171] A. Punge, S. O. Rizzoli, R. Jahn, J. D. Wildanger, L. Meyer, A. Schönle, L. Kastrup, S. W. Hell, *Microsc. Res. Tech.* **2008**, *71*, 644 – 650.
[172] V. Westphal, S. Hell, *Phys. Rev. Lett.* **2005**, *94, 143903*.
[173] L. Kastrup, S. W. Hell, *Angew. Chem.* **2004**, *116*, 6814 – 6818; *Angew. Chem. Int. Ed.* **2004**, *43*, 6646 – 6649.
[174] O. Griesbeck, G. S. Baird, R. E. Campbell, D. A. Zacharias, R. Y. Tsien, *J. Biol. Chem.* **2001**, *276*, 29188 – 29194.

Received: December 9, 2011
Published online on February 28, 2012

